Title

Phenotypic Screening Using High-Content Imaging to Identify Lysosomal pH Modulators in a Neuronal Cell Model

Journal

ACS Chemical Neuroscience, 13(10)

ISSN

1948-7193

Authors

Chin, Marcus Y
Ang, Kean-Hooi
Davies, Julia
et al.

Publication Date

2022-05-18

DOI

10.1021/acschemneuro.1c00804

Peer reviewed

ACS Chemical Neuroscience

pubs.acs.org/chemneuro

Research Article

Phenotypic Screening Using High-Content Imaging to Identify Lysosomal pH Modulators in a Neuronal Cell Model

Marcus Y. Chin, Kean-Hooi Ang, Julia Davies, Carolina Alquezar, Virginia G. Garda, Brendan Rooney, Kun Leng, Martin Kampmann, Michelle R. Arkin,* and Aimee W. Kao*

Cite This: *ACS Chem. Neurosci.* 2022, 13, 1505−1516

Read Online

ACCESS | Metrics & More | Article Recommendations | Supporting Information

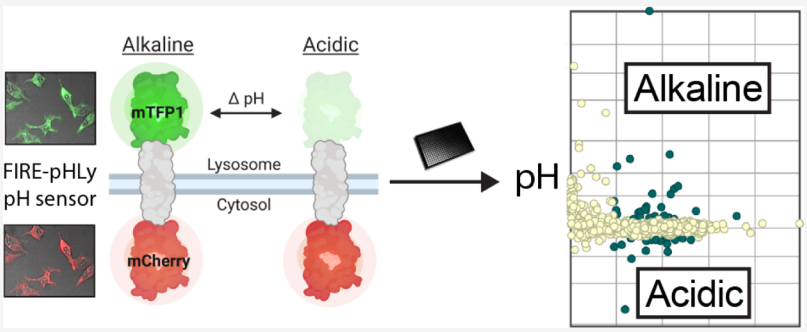

ABSTRACT: Lysosomes are intracellular organelles responsible for the degradation of diverse macromolecules in a cell. A highly acidic pH is required for the optimal functioning of lysosomal enzymes. Loss of lysosomal intralumenal acidity can disrupt cellular protein homeostasis and is linked to age-related diseases such as neurodegeneration. Using a new robust lysosomal pH biosensor (FIRE-pHLy), we developed a cell-based fluorescence assay for high-throughput screening (HTS) and applied it to differentiated SH-SY5Y neuroblastoma cells. The goal of this study was twofold: (1) to screen for small molecules that acidify lysosomal pH and (2) to identify molecular targets and pathways that regulate lysosomal pH. We conducted a screen of 1835 bioactive compounds with annotated target information to identify lysosomal pH modulators (both acidifiers and alkalinizers). Forty-five compounds passed the initial hit selection criteria, using a combined analysis approach of population-based and object-based data. Twenty-three compounds were retested in dose-response assays and two compounds, OSI-027 and PP242, were identified as top acidifying hits. Overall, data from this phenotypic HTS screen may be used to explore novel regulatory pathways of lysosomal pH regulation. Additionally, OSI-027 and PP242 may serve as useful tool compounds to enable mechanistic studies of autophagy activation and lysosomal acidification as potential therapeutic pathways for neurodegenerative diseases.

KEYWORDS: *lysosomes, lysosomal pH, pH biosensor, high-content analysis, neurons, phenotypic screening*

1. INTRODUCTION

Lysosomes are specialized membrane-bound organelles that participate in many crucial cellular functions such as macromolecular degradation, nutrient sensing, and secretion.[1−3] They are intimately involved in autophagy, which serves as a key pathway for maintaining protein homeostasis within the cell. Lysosomes derive their degradative functions by possessing a very acidic lumen (pH ∼ 4.5−4.7),[4,5] allowing the optimal activation of hydrolytic enzymes that are ultimately responsible for substrate breakdown. The lysosomal pH is tightly regulated through the vacuolar-type H^+-ATPase (V-ATPase) proton pump and other counter-ion channels.[6]

Defective lysosomes are a common feature of age-related and neurodegenerative disorders. Numerous mutations have been found in genes directly involved in the endolysosomal pathway.[7,8] Pathological accumulation of proteins is also seen across various neurodegenerative diseases,[9,10] implicating a role in aberrant cellular clearance. While the exact mechanisms causing neurodegeneration remain elusive, these observations suggest an overall breakdown in protein homeostasis stemming from lysosomal dysfunction. Indeed, lysosomal acidity has been described to be impaired in studies of age-related neurodegenerative diseases.[11−16]

With increasing evidence underscoring its critical role in neurodegenerative diseases, correcting lysosomal function and pH regulation may be therapeutically tractable strategies for future drug development. However, relatively few phenotypic

Received: December 6, 2021
Accepted: April 25, 2022
Published: May 6, 2022

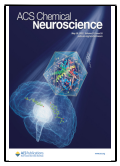

https://doi.org/10.1021/acschemneuro.1c00804
ACS Chem. Neurosci. 2022, 13, 1505−1516

screens have been conducted with a specific focus on lysosomes. High-throughput screening (HTS) studies have explored lysosomal morphology, positioning, and calcium regulation, with regard to lysosomal storage disorders and cancer.[17] Importantly, to our knowledge, no group has conducted a phenotypic screen on lysosomal pH. Such is the focus in the current study.

Novel lysosomal pH probes that specifically target lysosomes and accurately measure intralumenal pH have been described by various groups.[17−20] Recently, we engineered FIRE-pHLy, a genetically encoded ratiometric lysosomal pH biosensor with a reported pK_a of ∼4.4.[20,21] FIRE-pHLy presents advantages in automated, HTS, including stable expression in cells, accurate targeting to lysosomal compartments, and resistance to fluorescence quenching during fixation. Here, we utilized FIRE-pHLy to develop a cell-based phenotypic assay to identify small molecules that affect lysosomal pH. Ultimately, the modulation of lysosomal acidity may restore protein homeostasis defects and serve as a novel therapeutic strategy for neurodegenerative disease-related drug discovery.

2. RESULTS AND DISCUSSION

2.1. High-Content Imaging Screen to Identify Modulators of Lysosomal pH. To identify small molecules and biological pathways that regulate lysosomal pH, we developed a cell-based high-content imaging screen that measured relative changes in intralumenal pH of lysosomes through fluorescence detection (Figure 1). We utilized the

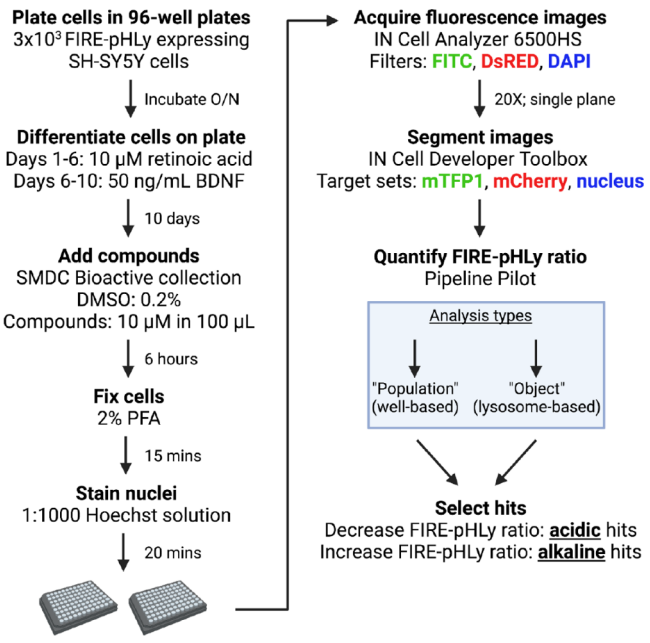

Figure 1. HTS flowchart for identifying lysosomal pH modulators.

previously validated genetically encoded pH biosensor, FIRE-pHLy or fluorescence indicator reporting pH of lysosomes.[21] FIRE-pHLy is composed of monomeric teal fluorescent protein 1 (mTFP1), mCherry, and lysosomal associated membrane protein 1 (LAMP1) that targets the fusion protein to lysosomal membranes. The fluorescence of mTFP1 is pH-dependent, while mCherry serves as an expression control and internal lysosome marker. Ratiometric imaging of mTFP1 and mCherry reports relative changes (herein referred to as the FIRE-pHLy ratio or mTFP1/mCherry) in the lysosomal pH environment.

FIRE-pHLy expressing SH-SY5Y cells were differentiated on 96-well microplates for 10 days and treated with bioactive compounds [10 μM/0.2% dimethyl sulfoxide (DMSO)] for their potential ability to decrease (acidify) or increase (alkalinize) lysosomal pH, as measured by the change in the FIRE-pHLy ratio. Compound ratios were calculated through the ratiometric quantification of mTFP1 and mCherry fluorescence intensities. Data was analyzed in parallel through two distinct pipelines (population-based and object-based quantification) and compared to select hits.

FIRE-pHLy can be stably expressed in a variety of cell models including human neuroblastoma SH-SY5Y cells,[21] which were selected for this HTS study due to their ability to be differentiated into neuron-like cells.[22] Because terminally differentiated SH-SY5Y cells have qualities appropriate to model aspects of neurodegenerative diseases, including endogenous expression of the aggregation-prone proteins such as tau,[23,24] they may provide enhanced therapeutic relevance over actively dividing cells in drug screening campaigns. Morphologically, undifferentiated cells are non-polarized with shortened processes, while their differentiated counterparts exhibit elongated and branching neurites extending from the cell body. Lysosomes are found both as perinuclear clusters within the cell body and as more individual entities along the processes of neurons, both of which we observed using FIRE-pHLY visualization.[21]

Cells were differentiated within 96-well microplates and then treated with a 1835-member library of bioactive compounds at the UCSF small-molecule discovery center (SMDC) for 6 h. This time point was rationalized to capture small molecules that changed lysosomal pH through fast-acting mechanisms (e.g., ion channels and transporters that generated the proton gradient) while avoiding longer-term global changes such as cellular proliferation and survival that could have non-specifically impacted lysosomal activity. The final screening concentration was 10 μM with a DMSO concentration of 0.2%, which did not artificially alter FIRE-pHLy ratio measurements (Figure S1A) and was non-toxic to cells (Figure S1B). Single plane images were acquired and analyzed through a custom segmentation protocol for mTFP1, mCherry and nuclei target sets (Figure 1).[21]

First, we designed a population-based analysis approach that quantified the FIRE-pHLy ratio averaged across the entire well. Given that there were no well-validated compounds that decreased lysosomal pH, we established variability in the screening data by the percent coefficient of variation (CV) of the FIRE-pHLy ratio. A CV of 5% in negative controls indicated that the assay was consistent across all assay plates (Figure S1C), with a mean FIRE-pHLy ratio of 0.36 ± 0.02. The CV for cell count was also acceptable (CV = 22%) with a mean of 1,163 ± 261 quantified cells per well (Figure S1D). Compounds that decreased the FIRE-pHLy ratio (i.e. decreased pH) were considered acidic hits, while any that increased the FIRE-pHLy ratio (i.e. increased pH) were labeled alkaline hits.

As a secondary method for hit selection, we developed an object-based analysis approach in order to focus on lysosomes, optimize sensitivity, and account for different populations of lysosomes based on coordinate location[25−27] in the differentiated SH-SY5Y cells. FIRE-pHLy ratios from individually segmented lysosomes in the DMSO controls were binned

https://doi.org/10.1021/acschemneuro.1c00804
ACS Chem. Neurosci. 2022, 13, 1505−1516

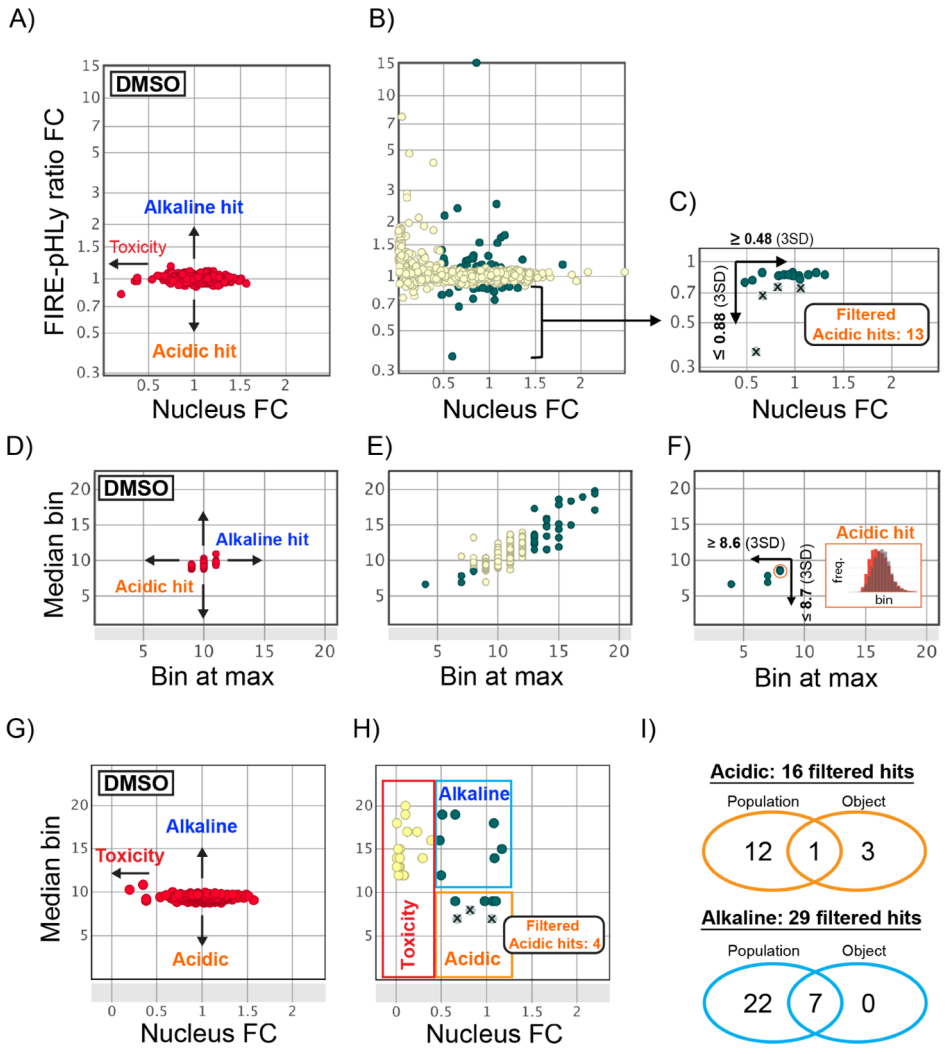

Figure 2. Hit selection for lysosomal acidifiers. (A–C) Population-based analysis. (A) 2D plot of FIRE-pHLy ratio FC versus nuclei FC (i.e., cell count) for all DMSO negative controls (shown in red dots; n = 384 wells across all assay plates). (B) 2D FIRE-pHLy ratio FC versus nuclei FC plot for all test compounds (n = 1 per compound; 1835 total compounds). Green dots represent primary hit compounds and yellow dots represent toxic or inactive compounds. (C) Expanded inset of acidic hits from Figure 2B. Acidic hits were selected using nucleus FC ≤ 3SD and FIRE-pHLy ratio FC ≤ 3SD compared to controls. Compounds that artificially altered the FIRE-pHLy ratio FC through mCherry fluorescence were excluded (green dots with black cross marks). (D–H) Lysosomal object-based analysis. (D) 2D plot of median bin versus bin at max for DMSO negative controls (shown in red dots; n = 384 wells across all assay plates). (E) 2D plot of median bin versus bin at max for all the test compounds (shown in yellow dots; n = 1 per compound; 1835 total compounds). Green dots represent primary hit compounds. (F) Lysosomal object-based acidic hits from Figure 2E. Acidic hits were selected using median bin ≤ 3SD and bin at max ≤ 3SD. (Inset) Frequency distribution for the hit compound highlighted with a red circle. Gray bars represent negative control distribution. Red bars represent hit compound distribution. (G) Filtering hits for cell toxicity. 2D plot of median bin versus nucleus FC for all DMSO negative controls. (H) 2D plot of median bin versus nucleus FC for test compounds. Compounds highlighted in the red box were excluded due to cell toxicity; alkaline hits are highlighted by the blue box; and acidic hits are highlighted in the orange box. Compounds that altered mCherry fluorescence were excluded (green dots with black cross marks). (I) Venn diagram showing the overlap of final filtered alkaline and acidic hits selected from population-based and lysosomal object-based analyses. Data in this figure was visualized in DataWarrior.

according to their ratio values, normalized from 0.0 to 1.0 with an increment of 0.05 per bin, and plotted as a histogram. FIRE-pHLy ratios from compound-treated wells were then normalized to the DMSO bins (see the Supporting Information). The data were normally distributed in the negative control DMSO-treated wells; assay means of "bin at max" and "median bin" were 9.88 ± 0.42 and 9.39 ± 0.24, respectively (Figure S1E). Shifts in the distribution caused by modulators of lysosomal pH would result in acidic (leftward curve shift) or alkaline (rightward curve shift) phenotypes; skew in the distribution could indicate that a subset of lysosomes were affected by compound treatment. The CVs of "bin at max" and "median bin" were 4 and 3%, supporting the consistency of our assay. Hits were selected from both population- and object-based approaches in tandem and compared to generate the primary hit list.

2.2. Primary Hit Selection, Filtering, and Comparison of Analysis Approaches. Thresholding for primary hits was performed using both parallel quantification pipelines, which will herein be referred to as "population-based analysis" (Figure 2A–C) and "object-based analysis" (Figure 2D–H). With population-based analysis, controls were visualized along a two-dimensional (2D) plot of FIRE-pHLy ratio fold change (FC) and nuclear count ("nucleus") FC to define the

https://doi.org/10.1021/acschemneuro.1c00804
ACS Chem. Neurosci. 2022, 13, 1505–1516

Table 1. Primary Filtered Acidifying Compounds Identified from Population-Based Analysis

Hit No.	SMDC ID	Compound	Ratio FC	Nuclei FC
1	972531	OSI-027[a]	0.88	0.98
2	972462	AZ 960	0.79	0.48
3	972875	3,4-Methylenedioxy-β-nitrostyrene	0.81	0.56
4	751824	Erlotinib	0.82	1.05
5	972846	LY2835219	0.85	0.98
6	131834	Nocodazole	0.85	1.04
7	972322	BMS-707035	0.85	0.83
8	972264	ABT-751 (E7010)	0.86	1.14
9	973076	Vinblastine	0.86	0.93
10	972537	Buparlisib	0.86	0.88
11	972406	Teniposide	0.86	1.31
12	972458	NVP-BHG712	0.88	1.22
13	130715	Nifedipine	0.88	0.66

[a]OSI-027 was identified as a hit in both population- and object-based analysis. Compounds highlighted in red passed dose-response retesting in differentiated SH-SH5Y cells.

Table 2. Primary Filtered Acidifying Compounds Identified from Object-Based Analysis

Hit No.	SMDC ID	Compound	Bin Median	Bin Max
1	972531	OSI-027[a]	8.50	8
2	972562	WAY-600	8.51	8
3	972465	PP242	8.66	8
4	972508	Ibrutinib	8.64	8

[a]OSI-027 was identified as a hit in both population- and object-based analysis. Compounds highlighted in red passed dose-response retesting in differentiated SH-SH5Y cells.

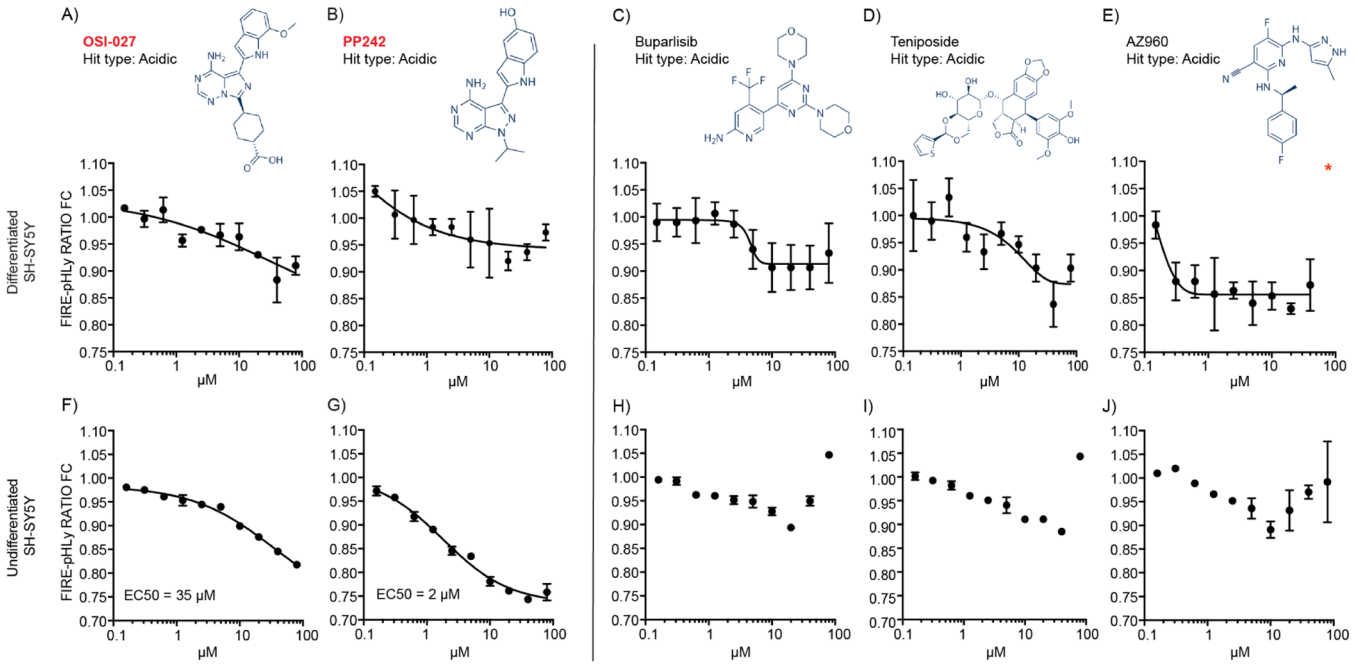

Figure 3. Top acidic hits tested in differentiated and undifferentiated SH-SY5Y cells.

boundaries for determining hits (Figure 2A). Compounds that exhibited a nucleus FC of less than 0.48 [−3 standard deviations; (SD)] were considered cytotoxic and excluded. Compounds with the FIRE-pHLy ratio FCs within ± 3SD of control were considered inactive (Figures 2B and S2A). Primary alkaline hits were identified based on the FIRE-pHLy ratio FC of at least 1.12 and nucleus FC of at least 0.48 (Figure S2B). Conversely, acidic hits were identified based on a FIRE-pHLy ratio FC of less than or equal to 0.88 and nucleus FC of at least 0.48 (Figure 2C). Importantly, we note that the FIRE-pHLy ratio could be artificially altered by changes in mCherry fluorescence. This may be caused by compound autofluorescence or off-target pH changes in the cytosolic environment where mCherry resides. To exclude these artifacts, a filter of mCherry fluorescence intensity FC was applied. Alkaline compounds with mCherry fluorescence FC > 0.7 and acidic compounds with FC < 1.5 were shortlisted. Overall, the population-based analysis approach identified 29 filtered alkaline hits (Figure S2B) and 13 filtered acidic hits (Figure 2C).

https://doi.org/10.1021/acschemneuro.1c00804
ACS Chem. Neurosci. 2022, 13, 1505−1516

A similar thresholding paradigm was used for object-based analysis. Compared to controls (Figure 2D), compounds that increased or decreased median bin and bin at max by 3SD were considered as hits (Figure 2E). Alkaline hits were selected based on a bin at the max and median of at least 13 and 11.5, respectively (Figure S2C). Acidic hits were identified based on a bin at the max and median of less than or equal to 8.7 and 8.6, respectively (Figure 2F). Subsequently, compounds that reduced nucleus FC compared to the control (Figure 2G,H) were eliminated. Finally, compounds that artificially altered mCherry fluorescence intensity were also removed (Figure 2H).

Hits were compiled from population-based and object-based analyses to generate the finalized filtered hit list. Thirteen acidic hits were identified from population-based analysis (Table 1), while four hits were identified from object-based analysis (Table 2). One compound, OSI-027, was found in both analysis pipelines. For alkaline hits, 29 compounds were identified from population-based methods (Table S1), 7 of which overlapped with object-based methods (Table S2). No additional alkaline hits were identified by object-based analysis. Overall, the population-based analysis method identified more hits than object-based analysis (Figure 2I) in both acidic and alkaline hit types. More alkalinizing hits were identified than acidifying hits.

2.3. Hit Confirmation with Dose-Response Retesting. Twenty-three compounds (i.e. all 16 acidic hits and the 7 alkaline hits identified in both population- and object-based analyses) were retested in a twofold dose response over a range of 80−0.156 μM in differentiated and undifferentiated SH-SY5Y cells. Undifferentiated cells were evaluated to support hit confirmation in differing cellular states. Among the 16 primary acidic hits, five compounds lowered lysosomal pH in a dose-dependent manner in differentiated cells (Figure 3A−E). Among these five primary hits, OSI-027 and PP242 reproduced in undifferentiated cells (Figure 3F,G). The estimated EC50 values for OSI-027 (Figure 3F) and PP242 (Figure 3G) in undifferentiated cells were 35 and 2 μM, respectively. The narrow range for differentiated SH-SY5Y cells makes it difficult to precisely measure EC50. The remaining three compounds—buparlisib, teniposide, and AZ960—exhibited marginal dose-response with a much narrower range in FIRE-pHLy ratio FC in undifferentiated cells (Figure 3H−J). We observed a FC reversal at higher doses for these compounds, which may be due to cell death. Finally, in the alkaline direction, reserpine robustly increased lysosomal pH, with a ∼8.3-fold decrease in EC50 post-differentiation (Figure S3).

Ten-point dose-response curves (2-fold serial dilution) from 0.15 to 80 μM. Cells were treated with compounds for 6 h before imaging. FIRE-pHLy ratios were taken from total mTFP1/mCherry fluorescence, displayed as a FC relative to control, and plotted according to dose. (A−E) Five primary hits tested in differentiated SH-SY5Y cells. (A) OSI-027. (B) PP242. (C) Buparlisib. (D) Teniposide. (E) AZ960. (F-J) Hits retested in undifferentiated cells. (F) OSI-027. (G) PP242. (H) Buparlisib. (I) Teniposide. (J) AZ960. OSI-027 and PP242, highlighted in red, yielded the strongest responses and were selected for further validation studies. Data points are presented as mean ± SD, from 3 biological replicates; n = ∼3000−5000 differentiated cells or ∼15,000−20,000 undifferentiated cells quantified per dose per time point. Dose-response curves were generated using a simple linear regression model from which EC50 values were estimated. Red asterisk: single data point not displayed within the Y-axis range.

Overall, we note the consistent expansion of the ratio FC range across the ten-point dose response in undifferentiated cells compared to their differentiated counterparts. In differentiated cells, the ratio FC range for OSI-027 and PP-242 was from ∼1.00 to ∼0.90 and ∼1.05 to ∼0.93, respectively. For the undifferentiated cells, the ranges for OSI-027 and PP242 were from ∼0.97 to ∼0.81 and ∼0.97 to ∼0.75, respectively. These data suggest that undifferentiated SH-SY5Y cells are more sensitive to pH lowering effects induced by OSI-027 and PP242 than differentiated cells. We elected to proceed with validating the top two acidic hits, OSI-027 and PP242, because of their chemical similarity and potential mechanistic interest in reacidifying lysosomes. The overall summary of the primary screen is detailed in Figure 4.

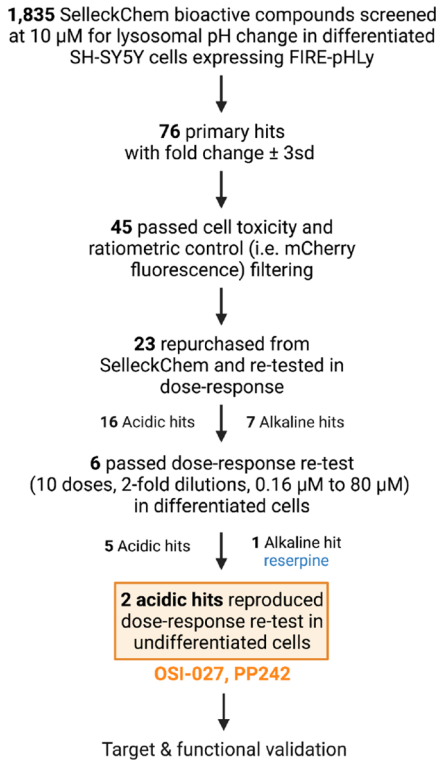

Figure 4. Hit selection summary. Summary of small molecule hits that modulate lysosomal pH in undifferentiated and differentiated SH-SY5Y cells.

2.4. Functional Validation of Top Acidic Hits OSI-027 and PP242. To functionally validate acidification of lysosomal pH, we treated live undifferentiated SH-SY5Y cells (without FIRE-pHLy) with compounds and assessed cathepsin D activity (Figure 5A). Because cathepsin D auto-activates at acidic pH,[28] its activity can be used as a functional readout of lysosomal pH; BODIPY FL-Pepstatin A is a cathepsin D antagonist that binds to the active form of the enzyme.[29] Cells were treated with OSI-027 and PP-242 at 10 μM for various times before BODIPY FL Pepstatin A fluorescence was assayed (Figure 5B). Compared to DMSO control, cathepsin D activity was significantly increased with OSI-027 and PP242 treatment. As a negative control, we tested bafilomycin A1 (BafA1), which increased pH by inhibiting the V-ATPase proton pump. BafA1 slightly decreased cathepsin D activity, but not

https://doi.org/10.1021/acschemneuro.1c00804
ACS Chem. Neurosci. 2022, 13, 1505−1516

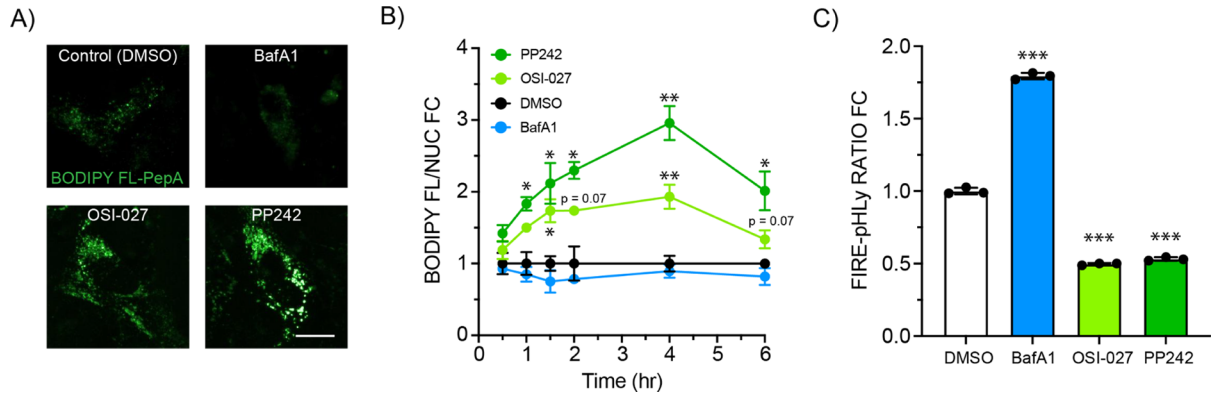

Figure 5. OSI-027 and PP242 increases mature cathepsin D levels in SH-SY5Y cells and acidifies pH in human iAstrocytes. (A) Representative fluorescence images of undifferentiated SH-SY5Y cells treated with DMSO, 100 nM BafA1, 10 μM OSI-027, and 10 μM PP242 at t = 6 h and stained with BODIPY FL Pepstatin A probe. Scale bar = 10 μm. (B) Time course of cells treated with compounds for 0.5, 1, 1.5, 2, 4, and 6 h. Cells were incubated with BODIPY FL Pepstatin A for 30 min before live-imaging. BODIPY FL fluorescence was normalized to cell number, displayed as a FC relative to control, and plotted against time (hours). Data points are presented as mean ± SD, from 3 biological replicates; n = ∼15,000−20,000 cells quantified per condition group per time point. Statistical analysis was performed using two-way ANOVA for multiple comparisons. *$p \leq 0.05$ and **$p \leq 0.01$. (C) Bar graph quantification of FIREpHLy ratio fold-change (FC) in human iPSC-derived astrocytes (iAstrocytes) treated with OSI-027 and PP242 at 10 μM for 24 h. Data points are presented as median ± SD from three technical replicates. Statistical analysis was performed using one-way ANOVA for multiple comparisons. ***$p \leq 0.001$.

significantly, suggesting that the alkalinization of lysosomes did not further lower basal activated enzyme levels. Overall, the correlation between the FIRE-pHLy ratio FC decrease and cathepsin D level increase validated OSI-027 and PP242 as robust—and functionally relevant—lysosomal pH acidifiers.

After confirming that OSI-027 and PP-242 acidified lysosomal pH and increased active cathepsin D levels, we sought to validate these compounds in another native cell model, namely, human-induced pluripotent stem cell (iPSC)-derived astrocytes, or iAstrocytes. Quiescent (non-reactive) iAstrocytes stably expressing FIRE-pHLy were subsequently treated for 24 h with OSI-027 and PP242 (Figure 5C). Both compounds acidified pH in iAstrocytes compared to control treatment (∼50% reduction in FIRE-pHLy ratio FC), providing further support that these compounds acidified lysosomes across multiple cell types.

Reactive astrocytes secrete neurotoxic factors and have been implicated in the neuroinflammatory pathogenesis of neurodegenerative diseases.[30] Recently, Rooney et al. described an in vitro system to model inflammatory reactive astrocytes.[31,32] Reactive iAstrocytes activated by cytokines exhibited an alkaline lysosomal pH, which was accompanied by increased levels of lysosomal exocytosis, a contributor to neurotoxicity.[32] When reactive iAstrocytes were treated with 10 μM of PP242, elevated lysosomal pH was restored to control levels and was accompanied by a reduction in lysosomal exocytosis.[32] Ultimately, these data supported the notion that aberrant lysosomal pH was a contributing factor to neuroinflammation-induced functional changes in neurodegenerative disease and may be corrected with small molecules such as PP242 and OSI-027. Taken together, the acidifying effect of OSI-027 and PP242 in lysosomes was recapitulated in disease models. We posit that its effects may be therapeutic in other contexts of lysosomal dysfunction.

2.5. OSI-027 and PP242 Inhibit mTOR and Induce Autophagy in SH-SY5Y Cells. Both OSI-027 and PP242 are described as potent and selective ATP-competitive inhibitors of mammalian target of rapamycin (mTOR).[33−35] mTOR forms two protein complexes, mTORC1 and mTORC2; these signaling complexes (Figure 6A) form a major hub that regulates cellular processes such as metabolism, growth, and proliferation. mTOR inhibition is coupled with autophagy induction, which is associated with lysosomal activation and acidification.[36−38]

To understand whether the lysosomal acidification promoted by OSI-027 and PP242 was related to their role as mTOR inhibitors, we assessed mTOR inhibition and autophagy activation (Figure 6). Both compounds dose dependently inhibited downstream targets of mTORC1 (Figure 6B,D) and mTORC2 (Figure 6B,E) in undifferentiated SH-SY5Y cells. mTORC1 activity was measured by the phosphorylation state of P70 S6 Kinase (P70S6K) at position Thr389 and mTORC2 activity was assessed by the phosphorylation of Akt at position Ser473.

After confirming that OSI-027 and PP242 inhibited mTOR, we measured their ability to activate autophagy. mTORC1 negatively regulates autophagy through the phosphorylation of Unc-51-like autophagy activating kinase (ULK1) at Ser757.[39] OSI-027 and PP242 reduced ULK1^{Ser757} levels dose dependently with near complete reduction at 10 μM (Figure 6C,F), suggesting that both drugs initiated mTORC1-dependent autophagy. We then measured the levels of microtubule-associated protein light chain 3B (LC3B). The conversion of LC3B-I to LC3B-II correlates with the number of formed autophagosomes and therefore reflects autophagy activation.[40,41] The ratio of LC3B-II to LC3B-I increased at higher OSI-027 and PP242 doses, achieving significance at 10 μM (Figure 6C,G). Finally, we tested for p62, which is an autophagic cargo adaptor that is shuttled into lysosomes during autophagy for degradation.[42] Corroborating our data above, PP242 treatment lowered p62 protein levels, while OSI-027 trended to decreased p62 levels, although this result was not statistically significant (Figure 6C,H). Together, these results demonstrated that OSI-027 and PP242 induced autophagy, indicating that their ability to acidify lysosomes may be secondary to the induction of autophagy rather than a direct action on the lysosome.

2.6. OSI-027 and PP242 Acidifies Lysosomes More Potently than Other mTOR Inhibitors. Interestingly, our compound screen included other mTOR inhibitors, such as

https://doi.org/10.1021/acschemneuro.1c00804
ACS Chem. Neurosci. 2022, 13, 1505−1516

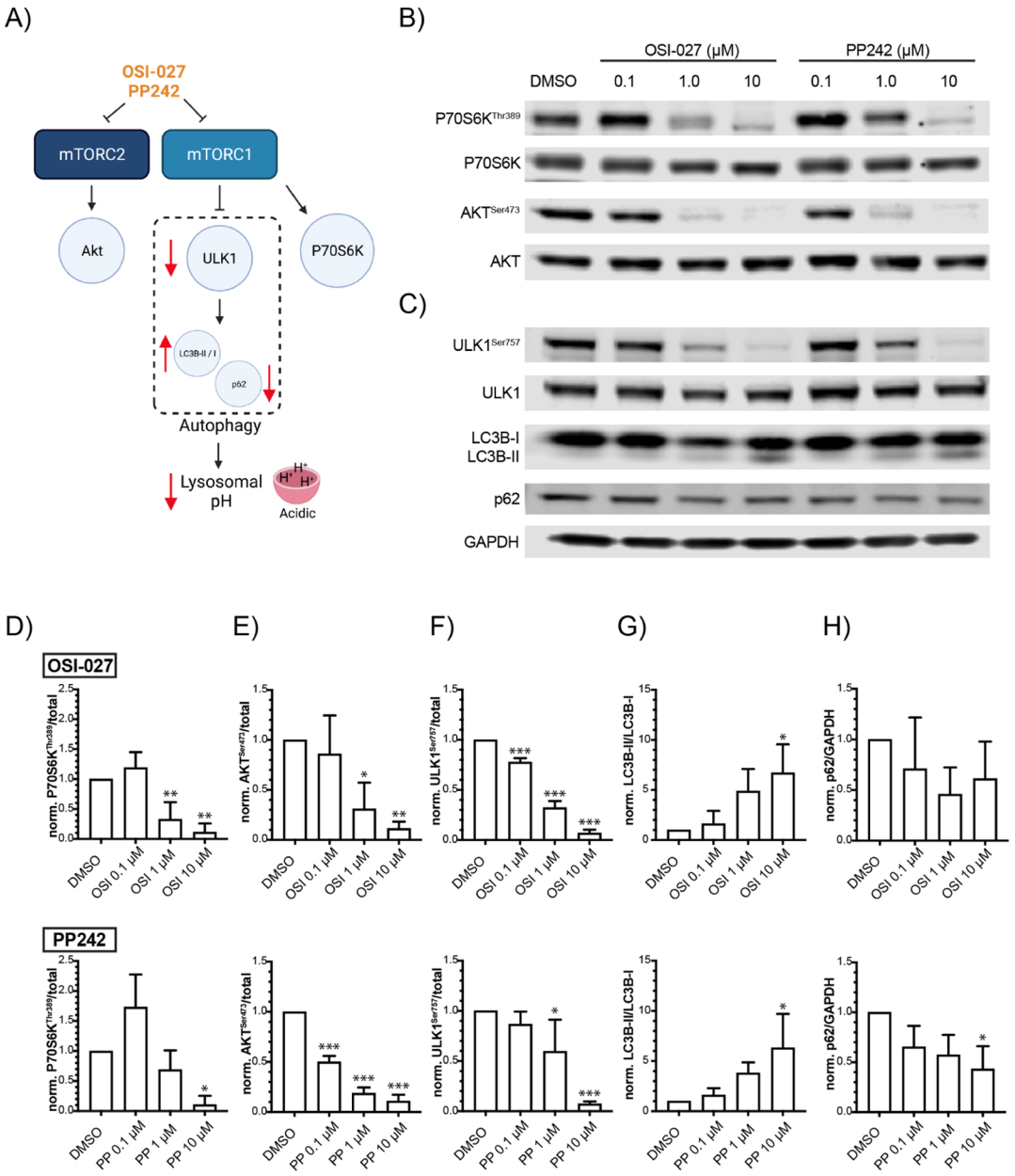

Figure 6. OSI-027 and PP242 inhibits mTORC1/2 and activates autophagy markers. (A) Simplified schematic of the proposed mechanism for OSI-027 and PP242-mediated lysosomal acidification through autophagy (highlighted in red arrows). Compounds are shown in orange. (B) Representative immunoblots for mTORC1 and mTORC2 phosphorylation substrates P70S6K^{Thr389} and Akt^{Ser473}, respectively, in FIRE-pHLy SH-SY5Y cells treated with OSI-027 and PP242 at 0.1, 1, and 10 μM. (C) Representative immunoblots for autophagy markers ULK1^{Ser757}, LC3B-I/LC3B-II, and p62 respectively, in FIRE-pHLy SH-SY5Y cells treated with OSI-027 (OSI) and PP242 (PP) (same as above). GAPDH was used as the housekeeping protein. Note: WT SH-SY5Y cells were used to generate the p62 immunoblots. (D) Bar graphs showing quantification of P70S6K^{Thr389}/total (E) Akt^{Ser473}/total, (F) ULK1^{Ser757}/total, (G) LC3B-II/LC3B-I, and (H) p62/GAPDH. OSI-027 shown in the top row and PP242 shown in the bottom row. Data is normalized to DMSO controls. Bars are presented as mean ± SD from three independent replicates. Statistical analysis was performed using one-way ANOVA for multiple comparisons. *$p \leq 0.05$; **$p \leq 0.01$; ***$p \leq 0.001$.

rapamycin and torin1, that were not identified as primary hits in our screen. To assess the differential effectiveness of additional mTOR inhibitors in modulating lysosomal pH, we retested rapamycin and torin 1 in undifferentiated FIRE-pHLy expressing SH-SY5Y cells over 24 h (Figure 7). Confirming our screening results, OSI-027 and PP242 treatment induced a dose- and time-dependent decrease in lysosomal pH in cells (Figure 7A,B), but treatment with rapamycin and torin1 did not acidify lysosomes across the tested dose range up to 24 h (Figure 7C,D). These results suggested that at the dosage and timing used in these experiments, OSI-027 and PP242 were more effective in acidifying lysosomal pH in undifferentiated SH-SY5Y cells than the mTOR inhibitors torin1 and rapamycin.

Because we proposed that OSI-027 and PP242 induced pH acidification by activating autophagy, we hypothesized that rapamycin and torin1 did not activate autophagy in SH-SY5Y cells, at the doses and timings used in this study. Indeed, though we confirmed that these compounds inhibited mTORC (Figure S4A), rapamycin did not significantly reduce ULK1^{Ser757} levels nor increase the ratio of LC3B-I and LC3B-II, indicating that autophagy was not activated under these

https://doi.org/10.1021/acschemneuro.1c00804
ACS Chem. Neurosci. 2022, 13, 1505−1516

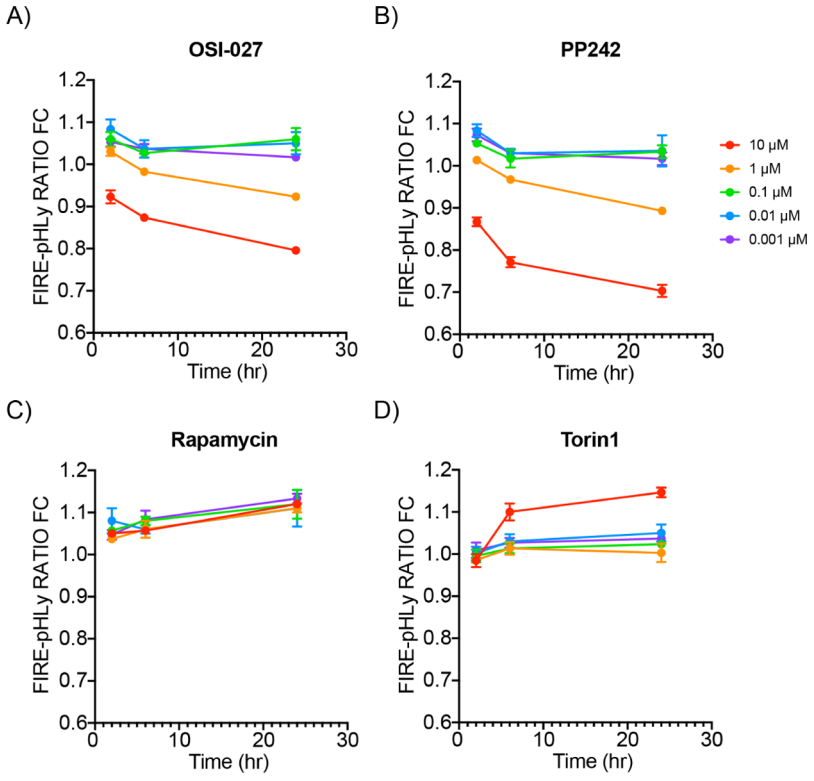

Figure 7. Dose-response and time-course comparison of mTOR inhibitors on lysosomal acidification. Five-point dose response (10-fold serial dilution) from 0.0001 to 10 μM treatment of (A) OSI-027, (B) PP242, (C) Rapamycin, and (D) Torin1 measured after 2, 6, and 24 h in undifferentiated FIRE-pHLy expressing SH-SY5Y cells. FIRE-pHLy ratio measurements were normalized to dose- and time-matched controls. Data points are presented as mean ± SD, from 3 technical replicates; n = ∼15,000−20,000 cells quantified per condition group per time point.

conditions (Figure S4A). Although torin1 treatment did reduce ULK1^{Ser757} levels starting at 100 nM compound, it did not significantly increase the LC3B-II/LC3B-I ratio (Figure S4B), suggesting that torin1 did not induce autophagy in as strongly as OSI-027 and PP242.

In summary, we performed a high-content imaging-based phenotypic screen to identify small molecules that modulate lysosomal pH with a specific focus on acidifying compounds. We identified 16 acidic and twenty29 alkaline compounds using two distinct hit selection approaches. Population-based analysis is used in standard plate-based HTS studies, while object-based analysis provides a novel technique that could be used in future studies to dissect organelle subpopulation phenotypes. While the latter technique yielded an overall lower acidic hit rate, the validation rate was superior to population-based analysis. Out of the four acidic hits identified using the object-based approach, two were confirmed as top hits and validated in subsequent orthogonal assays. Indeed, we were able to visualize more nuanced changes in the distribution of lysosomes according to their pH, which improves upon existing analysis methods of image-based cellular assays.

Ultimately, we validated 2 out of the 16 primary acidic hits. This hit rate may be a product of both biological factors such as lysosomal pH dynamics and screening limitations such as the library size and protein druggability of the target(s). We speculate that because basal lumenal pH of lysosomes is already highly acidic (∼4.5) compared to other cellular compartments, acidification beyond this set-point may be tightly regulated or even perhaps detrimental to the cell in certain contexts. This may explain the reduced dynamic range of FIRE-pHLy signal exhibited by acidifiers compared to alkalinizing compounds. Indeed, only a few examples highlight specific roles of lysosomal hyper-acidification in melanosome trafficking[43] and phospholipid biosynthesis.[44]

Alkaline compartments, on the other hand, are more common in the cell. In fact, lysosomes mature from the endolysosomal network, which maintains more alkaline pH ranges. Exogenous agents, such as drugs, have also been known to accumulate in acidic vesicles, such as lysosomes, and affect the local pH.[45,46] It is conceivable that perturbations in the alkaline direction are generally better tolerated in the cell (at least over short time periods), supporting our observation that alkalinizing compounds exhibited a larger signal range in the primary screen.

OSI-027 and PP242 were identified as top acidic hits, demonstrating lysosomal pH lowering effects in undifferentiated and differentiated SH-SY5Y neuronal-like cells and in basal and activated iAstrocytes, possibly through activation of autophagy. Indeed, other groups have utilized OSI-027 and PP242 to study autophagy in the context of neurodegenerative disease models. For example, Silva et al. identified OSI-027 as a top hit in a mutant tau protein lowering screen performed in patient iPSC-derived neurons.[47] Consistent with our data, OSI-027 lowered total mutant tau^{A152T} and hyperphosphorylated tau^{Ser396} levels at 1 and 10 μM, suggesting the correlation between lysosomal acidification and enhanced tau clearance. Interestingly, the tau lowering effect for OSI-027 was much stronger than that of rapamycin. Moreover, one group showed in a Parkinson's disease neuroinflammation model that impaired lysosomal acidification was accompanied by alpha-synuclein accumulation.[48] Treatment with 40 nM PP242 rescued lysosomal acidity as measured by LysoTracker dye and

https://doi.org/10.1021/acschemneuro.1c00804
ACS Chem. Neurosci. 2022, 13, 1505−1516

normalized alpha-synuclein protein levels in mouse PC12 cells and primary midbrain neurons. Together, these data support the supposition that OSI-027 and PP242 acidify lysosomes and thereby restore normal degradative function in neuronal cells.

The link between lysosomal acidification defects and clinical phenotypes, such as changes in the lysosomal morphology, remains an unstudied question in the field. To begin to understand this connection, high-resolution imaging techniques such as electron microscopy (EM) may be used. Past studies have already described EM as a robust method to visualize defective lysosomes in the context of lysosomal storage disorders and autophagy.[49,50] Conceivably compounds that rescue lysosomal functions through acidification such as OSI-027 and PP242 may also reverse abnormal morphologies.

It is still not entirely clear why OSI-027 and PP242 are more effective in activating autophagy and decreasing lysosomal pH than other mTOR inhibitors such as torin1 and rapamycin. It is plausible that OSI-027 and PP242 have undescribed targets independent of mTOR that may be contributing to autophagy and lysosomal acidity. In order to investigate additional targets, we measured ULK1^{Ser555} phosphorylation (Figure S5A). ULK1^{Ser555} is a mTOR-independent phosphosite controlled by AMP-activated protein kinase (AMPK) activity.[51] OSI-027 (Figure S5B) and rapamycin (Figure S5D) did not lower phosphorylated ULK1^{Ser555}/total levels, while a significant reduction was observed for PP242 (Figure S5C) at 10 μM and torin1 (Figure S5E) at 1 and 10 μM. Because these two compounds had differential effects on lysosomal acidification, we concluded that this particular non-mTOR phosphosite was unlikely to affect pH.

Nevertheless, kinase inhibitors are likely to have additional targets. According to the KINOMEscan database,[52] an assay platform that annotates competitive binding between inhibitors and a panel of known kinases, PP242 binds to multiple other kinases. These include phosphoinositide 3-kinase and ABL proto-oncogene 1, which have reported roles in regulating autophagy from cancer studies.[53−56] Thus, by evaluating the other targets of OSI-027 and PP242, one may identify additional, mTOR-independent, mechanisms of lysosomal acidification. Importantly, OSI-027 and PP242 may serve as "tool" compounds for the further investigation of the mechanisms driving autophagy-mediated lysosomal activation in the context of neurodegenerative diseases.

3. METHODS

3.1. Compound Library and Repurchased Compounds. The library consisted of 1835 compounds assembled from the commercially available SelleckChem bioactive collection (SelleckChem, Houston, TX). For dose-response and further validations, compounds were repurchased from SelleckChem, unless otherwise indicated. Repurchased compounds were evaluated for purity by liquid chromatography/mass spectrometry.

3.2. Cell Line Maintenance and Differentiation in 96-Well Microplates. Human WT and stably expressing FIRE-pHLy SH-SY5Y neuroblastoma cells[21] were maintained in 1:1 Eagle's minimum essential medium (ATCC, #30-003) and F12 medium (Life Technologies; Carlsbad, CA, #11765062) with 10% fetal bovine serum (FBS) and 1% pen/strep under standard humidified conditions of 37 °C and 5% CO_2 atmosphere.[21] Cells were trypsinized with 0.25% trypsin/EDTA solution (Sigma, #T4049) and seeded into collagen type-I-coated μClear 96-well microplates (Greiner Bio-One, #655956) at a low density of 10,000 cells/cm^2 with a total well volume of 100 μL using a WellMate microplate dispenser (Thermo Scientific, Waltham, MA) to allow for proliferation during the first phase of differentiation. Plates were incubated overnight at 37 °C/5% CO_2 before the start of differentiation, as previously described.[21] Briefly, cells were maintained in FBS(+) media supplemented with 10 μM retinoic acid from days 0 to 6 and FBS-free media supplemented with a 50 ng/mL brain-derived growth factor until compound pinning on day 10.

3.3. HTS Ratiometric FIRE-pHLy Lysosomal pH Reporter Assay. The drug screen was performed at the UCSF SMDC. From the library plate (5 mM stock dissolved in DMSO), 200 nL of the compound was added in singlicate to 96-well assay plates (10 μM final screening concentration) using a fixed-volume pin tool (V&P Scientific, San Diego, CA) loaded onto the BioMek-FXP liquid handling automation workstation (Beckman Coulter, Brea, CA). DMSO was added to negative control wells on every assay plate. Assay plates were incubated for 6 h (37 °C and 5% CO_2). 50 μL of 6% PFA (diluted in serum-free media) was dispensed directly into each 100 μL assay well (2% PFA final concentration) and shaken briefly using an EL406 Combination Washer Dispenser (BioTek, Winooski, VT). Plates were fixed at room temperature (RT) for 15 min and washed once with 100 μL 1× D-PBS (with $MgCl_2$ and $CaCl_2$). Cells were stained with 1:1000 (vol/well) Hoechst dye (10 mg/mL Hoechst 33342 solution, Thermo Fisher, #H3570) diluted in D-PBS for 20 min at RT protected from light and washed once with 1× D-PBS (with $MgCl_2$ and $CaCl_2$). Plates were wrapped and stored at 4 °C protected from light.

3.4. High-Content Confocal Imaging, Analysis Types, and Data Output. Following our previously described imaging methods and feature extraction protocols,[21] assay plates were imaged (at a single *Z*-plane) on the IN Cell 6500 HS Analyzer (General Electric Life Sciences/Cytiva, Marlborough, MA) and quantified on the IN Cell Developer Toolbox v1.9 (GE Life Sciences/Cytiva). Both population- and object-based analysis were used to quantify primary screening imaging data. Population-based analysis was used to validate hits in subsequent dose-response and validation assays. A detailed description of population- and object-based image analysis is available in the Supporting Information.

3.5. BODIPY FL Pepstatin A Live-Cell Time Course Assay. Mature cathepsin D levels were assessed via BODIPY FL Pepstatin A staining on live cells. The staining protocol was performed according to the manufacturer's protocol.[29] Briefly, cells were seeded in 96-well plates, cultured overnight, and treated for 30, 60, 90, 120, 240, and 360 min with 100 nM bafilomycin A1, 10 μM OSI-027, 10 μM PP-242, and DMSO as the solvent control. Prior to imaging, cells were incubated for 30 min with a staining solution consisting of 1 μM BODIPY FL Pepstatin A and 1:1000 (vol/well) Hoescht nuclear dye. Cells were washed once with D-PBS and imaged live on an IN cell analyzer 6500 HS and processed according to an adapted protocol on IN Cell Developer Toolbox v1.9.

3.6. Immunoblotting. Western blots were performed as previously described.[21]

3.6.1. Primary Antibodies. Rabbit anti-ULK (1:1000, cell signaling, #8054).
Rabbit anti-ULK^{Ser757} (1:1000, cell signaling, #14202).
Rabbit anti-ULK^{Ser555} (1:1000, cell signaling, #5869).
Rabbit anti-p70S6K (1:1000, cell signaling, #2708).
Rabbit anti-P70S6K^{Thr389} (1:1000, cell signaling, #9234).
Rabbit anti-Akt (1:1000, cell signaling, #9272).
Rabbit anti-Akt^{Ser437} (1:1000, cell signaling, #4060).
Rabbit anti-LC3B (1:1000, Sigma, #L7543).
Mouse anti-SQSTM1/p62 (1:1000, Santa Cruz, #48402).
Mouse anti-GAPDH (1:5000, Abcam, #8245).

3.6.2. Secondary Antibodies. Donkey anti-Mouse Green (1:10,000, LICOR, #926-32212).
Donkey anti-Rabbit Green (1:10,000, LICOR, #926-32213).
Donkey anti-Rabbit Red (1:10,000, LICOR, #926-68073).

3.7. iAstrocyte Experiments. iAstrocytes were generated as detailed in Leng et al.[31] Day 20 iAstrocytes were plated in ScienCell Astrocyte Media (ScienCell Research Laboratories cat. no. 1801) at 20,000 cells/cm^2 on BioLite Cell Culture Treated 96-well plates (ThermoFisher Scientific cat. no. 12-556-008) coated with growth factor reduced, Phenol Red-Free, LDEV-Free Matrigel Basement

https://doi.org/10.1021/acschemneuro.1c00804
ACS Chem. Neurosci. 2022, 13, 1505−1516

Membrane Matrix (Corning cat. no. 356231) diluted 1:200 in DMEM/F12 (ThermoFisher Scientific cat. no. 11330032). iAstrocytes were transduced with FIRE-pHLy lentivirus at the time of plating. Full media changes with ScienCell Astrocyte Media were conducted on days 1, 3, and 5 after plating. On day 5, small-molecule compounds were diluted in media to 10 μM. After 24 h (i.e. on day 6 after plating), iAstrocytes were incubated with Accutase Cell Dissociation Reagent (ThermoFisher Scientific cat. no. A11105-01) for 10 min at 37 °C and diluted in Dulbecco's phosphate buffered saline (Milipore Sigma cat. no. D8537) for flow cytometry analysis.

Data from flow cytometry experiments were analyzed using FlowJo (version 10.7.1). FIRE-pHLy-positive populations were determined through live cell (SSC-A vs FSC-A), single cell (FSC-H vs FSC-A), and transduced (mCherry$^+$) gating strategies. FIRE-pHLy signal was quantified as the Median FITC-A/mCherry-A ratio for each well.

3.8. Data Presentation, Statistical Analysis, and Illustrations. Visualization of control and screening hit data was performed on the SMDC HiTS server and DataWarrior, an open-source cheminformatics tool. Pre-processing of data was organized in Microsoft Excel. Calculations of hit selection measurements was conducted on Pipeline Pilot (Biovia) (see the Supporting Information). Dose-response curves were generated using a simple linear regression model in GraphPad Prism 9. For validation experiments, all data were generated from randomly selected sample populations from at least three independent experiments represented unless otherwise mentioned in the corresponding figure legends. Statistical data were presented as mean ± S.D or S.E.M. Multiple comparisons between groups were analyzed by the one-way or two-way ANOVA test. All data plots and statistical analyses were performed using GraphPad Prism 9 with no samples excluded. Significant differences between experimental groups were indicated as $^*P < 0.05$; $^{**}P < 0.01$; and $^{***}P < 0.001$; only $P < 0.05$ was considered as statistically significant. NS = not significant. Immunoblot images and quantifications were acquired from Image Studio (LI-COR Biosciences). Cartoon schematics were created on Biorender.com. Figures were assembled on Adobe Illustrator and Adobe Photoshop.

■ ASSOCIATED CONTENT

Supporting Information

The Supporting Information is available free of charge at https://pubs.acs.org/doi/10.1021/acschemneuro.1c00804.

> Assay performance for negative controls, hit selection for lysosomal alkalinizers, hit confirmation for top alkaline hit, mTORC1/2 immunoblots of cells treated with rapamycin and torin1, ULK1^{Ser555} immunoblots of cells treated with mTOR inhibitors, and methods describing the population- and object-based analysis pipelines (PDF)

■ AUTHOR INFORMATION

Corresponding Authors

Michelle R. Arkin − *Small Molecule Discovery Center, Department of Pharmaceutical Chemistry, University of California, San Francisco, California 94143, United States;* orcid.org/0000-0002-9366-6770; Email: michelle.arkin@ucsf.edu

Aimee W. Kao − *Memory and Aging Center, Department of Neurology, University of California, San Francisco, California 94158, United States;* orcid.org/0000-0002-7686-7968; Email: aimee.kao@ucsf.edu

Authors

Marcus Y. Chin − *Memory and Aging Center, Department of Neurology, University of California, San Francisco, California 94158, United States; Small Molecule Discovery Center, Department of Pharmaceutical Chemistry, University of California, San Francisco, California 94143, United States;* orcid.org/0000-0002-7037-1603

Kean-Hooi Ang − *Small Molecule Discovery Center, Department of Pharmaceutical Chemistry, University of California, San Francisco, California 94143, United States*

Julia Davies − *Small Molecule Discovery Center, Department of Pharmaceutical Chemistry, University of California, San Francisco, California 94143, United States*

Carolina Alquezar − *Memory and Aging Center, Department of Neurology, University of California, San Francisco, California 94158, United States*

Virginia G. Garda − *Memory and Aging Center, Department of Neurology, University of California, San Francisco, California 94158, United States; Small Molecule Discovery Center, Department of Pharmaceutical Chemistry, University of California, San Francisco, California 94143, United States*

Brendan Rooney − *Institute for Neurodegenerative Diseases, Department of Biochemistry and Biophysics, University of California, San Francisco, California 94158, United States*

Kun Leng − *Institute for Neurodegenerative Diseases, Department of Biochemistry and Biophysics, Biomedical Sciences Graduate Program, and Medical Scientist Training Program, University of California, San Francisco, California 94158, United States*

Martin Kampmann − *Institute for Neurodegenerative Diseases, Department of Biochemistry and Biophysics, University of California, San Francisco, California 94158, United States;* orcid.org/0000-0002-3819-7019

Complete contact information is available at: https://pubs.acs.org/10.1021/acschemneuro.1c00804

Author Contributions

M.Y.C., M.R.A., and A.W.K. for conceptualization and design; M.Y.C., K.A., J.D., C.A., and V.G.G. for experimental design and data acquisition; B.R., K.L, and M.K. for conceptualization, design, and data acquisition of iAstrocyte experiments; all authors analyzed and interpreted data; M.Y.C., M.R.A., and A.W.K. wrote the manuscript; and all authors edited the manuscript.

Notes

The authors declare no competing financial interest.

The authors declare that all relevant data supporting the findings of this study are available within the paper. Any data or reagents can be obtained from the corresponding authors (M.R.A. and A.W.K.) and on reasonable request.

■ ACKNOWLEDGMENTS

We thank the UCSF SMDC for their assistance on drug screening procedures, data management, and storage. We also thank Deanna Kroetz for insights on drug screening and validation. Additionally, we thank members of the Kao and Arkin labs for their thoughtful discussions. This work has received support from the NIH/NIA (R01 AG055342 to A.W.K.; R01 AG062359 to M.K.; and F30 AG066418 to K.L.). Finally, this work was included in the dissertation of M.Y.C for the Pharmaceutical Sciences and Pharmacogenomics doctoral program at UCSF (https://escholarship.org/uc/item/3xs387n6).[20]

■ ABBREVIATIONS

FIRE-pHLy, Fluorescence Indicator REporting pH in Lysosomes; mTFP1, monomeric teal fluorescent protein; V-ATPase, vacuolar-type ATPase; LAMP1, lysosomal-associated membrane protein 1; BafA1, bafilomycin A1; iPSC, induced pluripotent stem cells; RA, retinoic acid; BDNF, brain-derived neurotrophic factor; HTS, high-throughput screening; FC, fold change; CV, coefficient of variation; EC50, half maximal effective concentration; DMSO, dimethyl sulfoxide; WT, wildtype; ATP, adenosine triphosphate; mTOR, mammalian target of rapamycin; mTORC, mTOR complex; ULK, unc-51-like autophagy activating kinase; LC3B, microtubule-associated protein light chain 3B; PI3K, phosphoinositide 3-kinase; ALB1, ABL proto-oncogene 1; AMP, activated protein kinase; AMPK, AMP-activated protein kinase

■ REFERENCES

(1) Ballabio, A.; Bonifacino, J. S. Lysosomes as Dynamic Regulators of Cell and Organismal Homeostasis. *Nat. Rev. Mol. Cell Biol.* **2020**, *21*, 101−118.

(2) Lawrence, R. E.; Zoncu, R. The Lysosome as a Cellular Centre for Signalling, Metabolism and Quality Control. *Nat. Cell Biol.* **2019**, *21*, 133−142.

(3) Mony, V. K.; Benjamin, S.; O'Rourke, E. J. A Lysosome-Centered View of Nutrient Homeostasis. *Autophagy* **2016**, *12*, 619−631.

(4) Casey, J. R.; Grinstein, S.; Orlowski, J. Sensors and Regulators of Intracellular PH. *Nat. Rev. Mol. Cell Biol.* **2010**, *11*, 50−61.

(5) Ohkuma, S. Use of Fluorescein Isothiocyanate-Dextran to Measure Proton Pumping in Lysosomes and Related Organelles. *Methods Enzymol.* **1989**, *174*, 131−154.

(6) Mindell, J. A. Lysosomal Acidification Mechanisms. *Annu. Rev. Physiol.* **2012**, *74*, 69−86.

(7) Koh, J.-Y.; Kim, H. N.; Hwang, J. J.; Kim, Y.-H.; Park, S. E. Lysosomal Dysfunction in Proteinopathic Neurodegenerative Disorders: Possible Therapeutic Roles of CAMP and Zinc. *Mol. Brain* **2019**, *12*, 18.

(8) Settembre, C.; Fraldi, A.; Medina, D. L.; Ballabio, A. Signals for the Lysosome: A Control Center for Cellular Clearance and Energy Metabolism. *Nat. Rev. Mol. Cell Biol.* **2013**, *14*, 283−296.

(9) Monaco, A.; Fraldi, A. Protein Aggregation and Dysfunction of Autophagy-Lysosomal Pathway: A Vicious Cycle in Lysosomal Storage Diseases. *Front. Mol. Neurosci.* **2020**, *13*, 37.

(10) Ross, C. A.; Poirier, M. A. Protein Aggregation and Neurodegenerative Disease. *Nat. Med.* **2004**, *10*, S10−S17.

(11) Baxi, K.; Ghavidel, A.; Waddell, B.; Harkness, T. A.; de Carvalho, C. E. Regulation of Lysosomal Function by the DAF-16 Forkhead Transcription Factor Couples Reproduction to Aging in Caenorhabditis Elegans. *Genetics* **2017**, *207*, 83−101.

(12) Colacurcio, D. J.; Nixon, R. A. Disorders of Lysosomal Acidification—The Emerging Role of v-ATPase in Aging and Neurodegenerative Disease. *Ageing Res. Rev.* **2016**, *32*, 75−88.

(13) Hughes, A. L.; Gottschling, D. E. An Early Age Increase in Vacuolar PH Limits Mitochondrial Function and Lifespan in Yeast. *Nature* **2012**, *492*, 261−265.

(14) Lee, J.-H.; McBrayer, M. K.; Wolfe, D. M.; Haslett, L. J.; Kumar, A.; Sato, Y.; Lie, P. P. Y.; Mohan, P.; Coffey, E. E.; Kompella, U.; Mitchell, C. H.; Lloyd-Evans, E.; Nixon, R. A. Presenilin 1 Maintains Lysosomal Ca2+ Homeostasis via TRPML1 by Regulating VATPase-Mediated Lysosome Acidification. *Cell Rep.* **2015**, *12*, 1430−1444.

(15) Sun, Y.; Li, M.; Zhao, D.; Li, X.; Yang, C.; Wang, X. Lysosome Activity Is Modulated by Multiple Longevity Pathways and Is Important for Lifespan Extension in C. Elegans. *Elife* **2020**, *9*, No. e55745.

(16) Tong, B. C.-K.; Wu, A. J.; Huang, A. S.; Dong, R.; Malampati, S.; Iyaswamy, A.; Krishnamoorthi, S.; Sreenivasmurthy, S. G.; Zhu, Z.; Su, C.; Liu, J.; Song, J.; Lu, J.-H.; Tan, J.; Pan, W.; Li, M.; Cheung, K.-H. Lysosomal TPCN (Two Pore Segment Channel) Inhibition Ameliorates Beta-Amyloid Pathology and Mitigates Memory Impairment in Alzheimer Disease. *Autophagy* **2021**, *18*, 624−642.

(17) Chin, M. Y.; Espinosa, J. A.; Pohan, G.; Markossian, S.; Arkin, M. R. Reimagining Dots and Dashes: Visualizing Structure and Function of Organelles for High-Content Imaging Analysis. *Cell Chem. Biol.* **2021**, *28*, 320−337.

(18) Ponsford, A. H.; Ryan, T. A.; Raimondi, A.; Cocucci, E.; Wycislo, S. A.; Fröhlich, F.; Swan, L. E.; Stagi, M. Live Imaging of Intra-Lysosome PH in Cell Lines and Primary Neuronal Culture Using a Novel Genetically Encoded Biosensor. *Autophagy* **2020**, *17*, 1500.

(19) Webb, B. A.; Aloisio, F. M.; Charafeddine, R. A.; Cook, J.; Wittmann, T.; Barber, D. L. PHLARE: A New Biosensor Reveals Decreased Lysosome PH in Cancer Cells. *MBoC* **2021**, *32*, 91.

(20) Chin, M. Y.-Y. *Exploring Lysosomal PH as a Therapeutic Strategy for Neurodegeneration*; UCSF, 2021.

(21) Chin, M. Y.; Patwardhan, A. R.; Ang, K.-H.; Wang, A. L.; Alquezar, C.; Welch, M.; Nguyen, P. T.; Grabe, M.; Molofsky, A. V.; Arkin, M. R.; Kao, A. W. Genetically Encoded, PH-Sensitive MTFP1 Biosensor for Probing Lysosomal PH. *ACS Sens.* **2021**, *6*, 2168.

(22) Encinas, M.; Iglesias, M.; Liu, Y.; Wang, H.; Muhaisen, A.; Ceña, V.; Gallego, C.; Comella, J. X. Sequential Treatment of SH-SY5Y Cells with Retinoic Acid and Brain-Derived Neurotrophic Factor Gives Rise to Fully Differentiated, Neurotrophic Factor-Dependent, Human Neuron-Like Cells. *J. Neurochem.* **2000**, *75*, 991−1003.

(23) Forster, J. I.; Köglsberger, S.; Trefois, C.; Boyd, O.; Baumuratov, A. S.; Buck, L.; Balling, R.; Antony, P. M. A. Characterization of Differentiated SH-SY5Y as Neuronal Screening Model Reveals Increased Oxidative Vulnerability. *J. Biomol. Screen* **2016**, *21*, 496−509.

(24) Xicoy, H.; Wieringa, B.; Martens, G. J. M. The SH-SY5Y Cell Line in Parkinson's Disease Research: A Systematic Review. *Mol. Neurodegener.* **2017**, *12*, 10.

(25) Bright, N. A.; Davis, L. J.; Luzio, J. P. Endolysosomes Are the Principal Intracellular Sites of Acid Hydrolase Activity. *Curr. Biol.* **2016**, *26*, 2233−2245.

(26) Cabukusta, B.; Neefjes, J. Mechanisms of Lysosomal Positioning and Movement. *Traffic* **2018**, *19*, 761−769.

(27) Johnson, D. E.; Ostrowski, P.; Jaumouillé, V.; Grinstein, S. The Position of Lysosomes within the Cell Determines Their Luminal PH. *J. Cell Biol.* **2016**, *212*, 677−692.

(28) Gulnik, S.; Baldwin, E. T.; Tarasova, N.; Erickson, J. Human Liver Cathepsin D. *J. Mol. Biol.* **1992**, *227*, 265−270.

(29) Chen, C.-S.; Chen, W.-N. U.; Zhou, M.; Arttamangkul, S.; Haugland, R. P. Probing the Cathepsin D Using a BODIPY FL−Pepstatin A: Applications in Fluorescence Polarization and Microscopy. *J. Biochem. Biophys. Methods* **2000**, *42*, 137−151.

(30) Phatnani, H.; Maniatis, T. Astrocytes in Neurodegenerative Disease. *Cold Spring Harbor Perspect. Biol.* **2015**, *7*, a020628.

(31) Leng, K.; Rooney, B.; Kim, H.; Xia, W.; Koontz, M.; Krawczyk, M.; Zhang, Y.; Ullian, E. M.; Fancy, S. P. J.; Schrag, M. S.; Lippmann, E. S.; Kampmann, M. CRISPRi Screens in Human Astrocytes Elucidate Regulators of Distinct Inflammatory Reactive States; preprint. *Neuroscience* **2021**, DOI: 10.1101/2021.08.23.457400.

(32) Rooney, B.; Leng, K.; McCarthy, F.; Rose, I. V. L.; Herrington, K. A.; Bax, S.; Chin, M. Y.; Fathi, S.; Leonetti, M.; Kao, A. W.; Elias, J. E.; Kampmann, M. MTOR Controls Neurotoxic Lysosome Exocytosis in Inflammatory Reactive Astrocytes; preprint. *Cell Biol.* **2021**, DOI: 10.1101/2021.09.11.459904.

(33) Apsel, B.; Blair, J. A.; Gonzalez, B.; Nazif, T. M.; Feldman, M. E.; Aizenstein, B.; Hoffman, R.; Williams, R. L.; Shokat, K. M.; Knight, Z. A. Targeted Polypharmacology: Discovery of Dual Inhibitors of Tyrosine and Phosphoinositide Kinases. *Nat. Chem. Biol.* **2008**, *4*, 691−699.

(34) Bhagwat, S. V.; Gokhale, P. C.; Crew, A. P.; Cooke, A.; Yao, Y.; Mantis, C.; Kahler, J.; Workman, J.; Bittner, M.; Dudkin, L.; Epstein,

https://doi.org/10.1021/acschemneuro.1c00804
ACS Chem. Neurosci. 2022, 13, 1505−1516

D. M.; Gibson, N. W.; Wild, R.; Arnold, L. D.; Houghton, P. J.; Pachter, J. A. Preclinical Characterization of OSI-027, a Potent and Selective Inhibitor of MTORC1 and MTORC2: Distinct from Rapamycin. *Mol. Cancer Ther.* **2011**, *10*, 1394−1406.
(35) Falcon, B. L.; Barr, S.; Gokhale, P. C.; Chou, J.; Fogarty, J.; Depeille, P.; Miglarese, M.; Epstein, D. M.; McDonald, D. M. Reduced VEGF Production, Angiogenesis, and Vascular Regrowth Contribute to the Antitumor Properties of Dual MTORC1/MTORC2 Inhibitors. *Cancer Res.* **2011**, *71*, 1573−1583.
(36) Kim, Y. C.; Guan, K.-L. MTOR: A Pharmacologic Target for Autophagy Regulation. *J. Clin. Invest.* **2015**, *125*, 25−32.
(37) Yim, W. W.-Y.; Mizushima, N. Lysosome Biology in Autophagy. *Cell Discov.* **2020**, *6*, 1−12.
(38) Zhou, J.; Tan, S.-H.; Nicolas, V.; Bauvy, C.; Yang, N.-D.; Zhang, J.; Xue, Y.; Codogno, P.; Shen, H.-M. Activation of Lysosomal Function in the Course of Autophagy via MTORC1 Suppression and Autophagosome-Lysosome Fusion. *Cell Res.* **2013**, *23*, 508−523.
(39) Jung, C. H.; Jun, C. B.; Ro, S.-H.; Kim, Y.-M.; Otto, N. M.; Cao, J.; Kundu, M.; Kim, D.-H. ULK-Atg13-FIP200 Complexes Mediate MTOR Signaling to the Autophagy Machinery. *Mol. Biol. Cell* **2009**, *20*, 1992−2003.
(40) Klionsky, D. J.; Abdelmohsen, K.; Abe, A.; Abedin, M. J.; Abeliovich, H.; Arozena, A. A.; Adachi, H.; Adams, C. M.; Adams, P. D.; et al. Guidelines for the Use and Interpretation of Assays for Monitoring Autophagy (3rd Edition). *Autophagy* **2016**, *12*, 1−222.
(41) Menzies, F. M.; Moreau, K.; Puri, C.; Renna, M.; Rubinsztein, D. C. Measurement of Autophagic Activity in Mammalian Cells. *Curr. Protoc. Cell Biol.* **2012**, *54*, 15.16.1−15.16.25.
(42) Bjørkøy, G.; Lamark, T.; Pankiv, S.; Øvervatn, A.; Brech, A.; Johansen, T. Monitoring Autophagic Degradation of P62/SQSTM1. *Methods Enzymol.* **2009**, *452*, 181−197.
(43) van der Poel, S.; Wolthoorn, J.; van den Heuvel, D.; Egmond, M.; Groux-Degroote, S.; Neumann, S.; Gerritsen, H.; van Meer, G.; Sprong, H. Hyperacidification of Trans-Golgi Network and Endo/Lysosomes in Melanocytes by Glucosylceramide-Dependent V-ATPase Activity. *Traffic* **2011**, *12*, 1634−1647.
(44) Lenk, G. M.; Park, Y. N.; Lemons, R.; Flynn, E.; Plank, M.; Frei, C. M.; Davis, M. J.; Gregorka, B.; Swanson, J. A.; Meisler, M. H.; Kitzman, J. O. CRISPR Knockout Screen Implicates Three Genes in Lysosome Function. *Sci. Rep.* **2019**, *9*, 9609.
(45) De Duve, C.; De Barsy, T.; Poole, B.; Trouet, A.; Tulkens, P.; Van Hoof, F. o. Lysosomotropic Agents. *Biochem. Pharmacol.* **1974**, *23*, 2495−2531.
(46) Kuzu, O. F.; Toprak, M.; Noory, M. A.; Robertson, G. P. Effect of Lysosomotropic Molecules on Cellular Homeostasis. *Pharmacol. Res.* **2017**, *117*, 177−184.
(47) Silva, M. C.; Nandi, G. A.; Tentarelli, S.; Gurrell, I. K.; Jamier, T.; Lucente, D.; Dickerson, B. C.; Brown, D. G.; Brandon, N. J.; Haggarty, S. J. Prolonged Tau Clearance and Stress Vulnerability Rescue by Pharmacological Activation of Autophagy in Tauopathy Neurons. *Nat. Commun.* **2020**, *11*, 3258.
(48) Wang, M.-X.; Cheng, X.-Y.; Jin, M.; Cao, Y.-L.; Yang, Y.-P.; Wang, J.-D.; Li, Q.; Wang, F.; Hu, L.-F.; Liu, C.-F. TNF Compromises Lysosome Acidification and Reduces α-Synuclein Degradation via Autophagy in Dopaminergic Cells. *Exp. Neurol.* **2015**, *271*, 112−121.
(49) Vogler, C.; Rosenberg, H. S.; Williams, J. C.; Butler, I.; Opitz, J. M.; Bernstein, J. Electron Microscopy in the Diagnosis of Lysosomal Storage Diseases. *Am. J. Med. Genet. Suppl.* **1987**, *28*, 243−255.
(50) Jung, M.; Choi, H.; Mun, J. Y. The Autophagy Research in Electron Microscopy. *Appl. Microsc.* **2019**, *49*, 11.
(51) Kim, J.; Kundu, M.; Viollet, B.; Guan, K.-L. AMPK and MTOR Regulate Autophagy through Direct Phosphorylation of Ulk1. *Nat. Cell Biol.* **2011**, *13*, 132−141.
(52) Fabian, M. A.; Biggs, W. H.; Treiber, D. K.; Atteridge, C. E.; Azimioara, M. D.; Benedetti, M. G.; Carter, T. A.; Ciceri, P.; Edeen, P. T.; Floyd, M.; Ford, J. M.; Galvin, M.; Gerlach, J. L.; Grotzfeld, R. M.; Herrgard, S.; Insko, D. E.; Insko, M. A.; Lai, A. G.; Lélias, J.-M.; Mehta, S. A.; Milanov, Z. V.; Velasco, A. M.; Wodicka, L. M.; Patel, H. K.; Zarrinkar, P. P.; Lockhart, D. J. A Small Molecule-Kinase Interaction Map for Clinical Kinase Inhibitors. *Nat. Biotechnol.* **2005**, *23*, 329−336.
(53) Elzinga, B. M.; Nyhan, M. J.; Crowley, L. C.; O'Donovan, T. R.; Cahill, M. R.; McKenna, S. L. Induction of Autophagy by Imatinib Sequesters Bcr-Abl in Autophagosomes and down-Regulates Bcr-Abl Protein. *Am. J. Hematol.* **2013**, *88*, 455−462.
(54) Iershov, A.; Nemazanyy, I.; Alkhoury, C.; Girard, M.; Barth, E.; Cagnard, N.; Montagner, A.; Chretien, D.; Rugarli, E. I.; Guillou, H.; Pende, M.; Panasyuk, G. The Class 3 PI3K Coordinates Autophagy and Mitochondrial Lipid Catabolism by Controlling Nuclear Receptor PPARα. *Nat. Commun.* **2019**, *10*, 1566.
(55) Wang, S.; Li, J.; Du, Y.; Xu, Y.; Wang, Y.; Zhang, Z.; Xu, Z.; Zeng, Y.; Mao, X.; Cao, B. The Class I PI3K Inhibitor S14161 Induces Autophagy in Malignant Blood Cells by Modulating the Beclin 1/Vps34 Complex. *J. Pharmacol. Sci.* **2017**, *134*, 197−202.
(56) Yogalingam, G.; Pendergast, A. M. Abl Kinases Regulate Autophagy by Promoting the Trafficking and Function of Lysosomal Components. *J. Biol. Chem.* **2008**, *283*, 35941−35953.

https://doi.org/10.1021/acschemneuro.1c00804
ACS Chem. Neurosci. 2022, 13, 1505−1516